

Anomalous dimensions for ϕ^n in scale invariant $d = 3$ theory

I. Jack¹ and D.R.T. Jones²

Dept. of Mathematical Sciences, University of Liverpool, Liverpool L69 3BX, UK

Abstract

Recently it was shown that the scaling dimension of the operator ϕ^n in scale-invariant $d = 3$ theory may be computed semiclassically, and this was verified to leading order (two loops) in perturbation theory at leading and subleading n . Here we extend this verification to six loops, once again at leading and subleading n . We then perform a similar exercise for a theory with a multiplet of real scalars and an $O(N)$ invariant hexic interaction. We also investigate the strong-coupling regime for this example.

¹dij@liverpool.ac.uk

²drtj@liverpool.ac.uk

1 Introduction

Renormalizable theories with scale invariant scalar self-interactions exist in four (ϕ^4), six (ϕ^3) and three (ϕ^6) dimensions. There has been considerable recent interest in the latter, in particular in theories involving complex scalar fields and a $U(1)$ invariance, with $(\phi^*\phi)^3$ -type interactions³. The anomalous dimension of the operator ϕ^n , γ_{ϕ^n} , was calculated at the two loop level (in usual perturbation theory in powers of coupling constant λ) in Ref. [5] for the $U(1)$ invariant pure scalar theory, and the result compared with a semiclassical calculation valid to all orders in the product λn ; following the lines of similar calculations in four dimensions [6]. Of particular interest in this context is large n , because large charge operators are of peculiar relevance in conformal field theory. Also, amplitudes corresponding to many external lines are increasingly relevant in particle physics phenomenology, as collider energies increase, so insights gained by the study of them in simpler theories is worthwhile in itself. Agreement was found in Ref. [5] between perturbative and semiclassical results at the level of the leading and sub-leading terms in an expansion in powers of $1/n$. Here we extend the straightforward perturbative calculation to the six loop level and once again obtain agreement with the semiclassical calculation for the two leading terms in the same expansion.

In Ref. [7], the calculations of Ref. [5] were extended from the $U(1)$ to the $O(N)$ case. Accordingly, we also perform our perturbative checks up to six loops for the semiclassical $O(N)$ result as well. Furthermore, the $U(1)$ semiclassical result was compared with an effective field theory valid at large λn . Accordingly we also examine the semiclassical $O(N)$ results at large charge and find that we can obtain exact results for the N -dependent part of the coefficients in a large-charge expansion.

The paper is organised as follows: In Section 2 we describe the semiclassical calculation in the $U(1)$ case, following Ref. [5], and then compare with the perturbative(i.e. small λn) results at four and six loops. In Section 3 we discuss the extension to the $O(N)$ case as in Ref. [7], and perform a similar perturbative comparison. In Section 4 we describe the large charge limit and show how to compute the N -dependent parts of the coefficients in the large charge expansion. We offer some concluding remarks in Section 5. Finally in the Appendix we give a pedagogical description of the various methods used in our computation of the four-loop and six-loop Feynman diagrams involved in our perturbative check.

³In Ref. [1], a $d = 3$ Chern-Simons gauge theory with such an interaction was studied, including also Yukawa couplings to a multiplet of fermions. From the two-loop β functions (previously calculated by Avdeev et al [2] [3]), persuasive evidence was presented for the existence of an a -theorem for such theories. This was subsequently confirmed by higher loop calculations in Ref. [4], with the scalar self-interaction replaced by a general hexic one with an arbitrary number of real scalar fields.

2 The $U(1)$ case

The lagrangian of the theory is

$$\mathcal{L} = \partial_\mu \phi^* \partial^\mu \phi + m^2 \phi^* \phi + \left(\frac{\lambda}{3!}\right)^2 (\phi^* \phi)^3 \quad (2.1)$$

We shall be using dimensional regularisation with $d = 3 - \epsilon$. The agreement between the semiclassical and perturbative results is expected to hold at the conformally invariant fixed point. However, because the β -function starts at two-loop order in $d = 3$, the theory is conformally invariant up to $\mathcal{O}(\lambda)$, and this is already sufficient for the agreement of the leading and subleading terms in n . The scaling dimension Δ_{ϕ^n} is expanded as (returning to general d for the present, in order to facilitate the later discussion of convergence issues)

$$\Delta_{\phi^n} = n \left(\frac{d}{2} - 1\right) + \gamma_{\phi^n} = \sum_{\kappa=-1} \lambda^\kappa \Delta_\kappa(\lambda n). \quad (2.2)$$

For the leading and subleading terms in n , knowledge of Δ_{-1} and Δ_0 is sufficient. The semiclassical computation is performed by mapping the theory via a Weyl transformation to a cylinder $\mathbb{R} \times S^{d-1}$, where S^{d-1} is a sphere of radius R ; where the $\mathcal{R}\phi^*\phi$ term (\mathcal{R} being the Ricci curvature) generates an effective $m^2\phi^*\phi$ mass term with $m = \frac{d-2}{2R}$. It was shown in Ref. [5] that stationary configurations of the action are characterised by a chemical potential μ ,

$$R\mu = \frac{1}{2\sqrt{2}} \sqrt{1 + \sqrt{1 + \frac{\lambda^2 n^2}{12\pi^2}}}. \quad (2.3)$$

It was further shown in Ref. [5] that Δ_{-1} may be written

$$\Delta_{-1}(\lambda n) = \lambda n F_{-1} \left(\frac{\lambda^2 n^2}{12\pi^2}\right), \quad (2.4)$$

where

$$F_{-1}(x) = \frac{1 + \sqrt{1+x} + \frac{x}{3}}{\sqrt{2}(1 + \sqrt{1+x})^{\frac{3}{2}}}. \quad (2.5)$$

(For convenience we give the results for $d = 3$ in Eqs. (2.3), (2.5).) Expanding to quadratic order around stationary configurations results in an action with two modes ω_\pm given by

$$\omega_\pm^2(l) = J_l^2 + 2(2\mu^2 - m^2) \pm 2\sqrt{J_l^2 \mu^2 + (2\mu^2 - m^2)^2}, \quad (2.6)$$

where

$$J_l^2 = \frac{l(l+d-2)}{R^2} \quad (2.7)$$

is the eigenvalue of the Laplacian on the sphere. The dispersion relation for ω_+ describes a “gapped” mode, while that for ω_- describes a “Type I” (relativistic) Goldstone boson [8]. The one-loop correction Δ_0 is then determined by the fluctuation determinant corresponding to this quadratic action, which is given by

$$\Delta_0(\lambda n) = \frac{R}{2} \sum_{l=0}^{\infty} n_l [\omega_+(l) + \omega_-(l) - 2\omega_0(l)], \quad (2.8)$$

where

$$\omega_0^2(l) = J_l^2 + m^2 = \frac{1}{R^2} \left(l + \frac{d-2}{2} \right)^2 \quad (2.9)$$

is the free theory dispersion relation,

$$n_l = \frac{(2l+d-2)\Gamma(l+d-2)}{\Gamma(l+1)\Gamma(d-1)} \quad (2.10)$$

is the multiplicity of the laplacian on the d -dimensional sphere, and where ω_{\pm} are defined in (2.6). It was shown in Ref. [5] that after analytic continuation to negative d , we may obtain a regularised form for Δ_0 convergent for $d \rightarrow 3$, and we obtain in $d = 3$

$$\Delta_0(\lambda n) = \frac{1}{4} - 3(R\mu)^2 + \frac{1}{2}\sqrt{8R^2\mu^2 - 1} + \frac{1}{2} \sum_{l=1}^{\infty} \sigma(l), \quad (2.11)$$

where μ , ω_{\pm} are given by Eqs. (2.3), (2.6) (with now $m = \frac{1}{2R}$) and where

$$\sigma(l) = (1+2l)R[\omega_+(l) + \omega_-(l)] - 4l(l+1) - \left(6R^2\mu^2 - \frac{1}{2} \right) \quad (2.12)$$

is defined by subtracting positive and zero powers of l in the large- l expansion of Eq. (2.8) so as to give a convergent sum. With a slight abuse of notation, we use the same notation $\Delta_0(\lambda n)$ for both the unregularised and regularised forms of the fluctuation operator.

Expanding $\sigma(l)$ in powers of $\frac{\lambda^2 n^2}{12\pi^2}$,

$$\sigma(l) = C_{2,l} \left(\frac{\lambda^2 n^2}{12\pi^2} \right)^2 + C_{3,l} \left(\frac{\lambda^2 n^2}{12\pi^2} \right)^3 + \dots, \quad (2.13)$$

where

$$C_{2,l} = -\frac{13l^2 + 13l + 1}{128l(l+1)(2l+1)^2},$$

$$C_{3,l} = \frac{208l^6 + 624l^5 + 747l^4 + 454l^3 + 138l^2 + 15l + 1}{1024l^2(l+1)^2(2l+1)^4}. \quad (2.14)$$

Using

$$\begin{aligned}\sum_{l=1}^{\infty} C_{2,l} &= \frac{1}{16} \left(1 - \frac{9}{64} \pi^2 \right), \\ \sum_{l=1}^{\infty} C_{3,l} &= \frac{1}{1024} \left(-47 + \frac{10}{3} \pi^2 + \frac{9}{32} \pi^4 \right),\end{aligned}\tag{2.15}$$

and combining Eqs. (2.2) (with now $d = 3$), (2.4), (2.11)-(2.15) we find the expansion

$$\begin{aligned}\Delta_{\phi^n} &= \frac{n}{2} + \kappa \left[\frac{n^3 - 3n^2}{9} + \mathcal{O}(n) \right] \\ &\quad - \kappa^2 \left[\frac{n^5}{9} - \frac{n^4(64 - 9\pi^2)}{72} + \mathcal{O}(n^3) \right] \\ &\quad + \kappa^3 \left[\frac{2n^7}{9} + \frac{2}{9} \left\{ -13 + \frac{10}{9} \pi^2 + \frac{3}{32} \pi^4 \right\} n^6 + \mathcal{O}(n^5) \right] + \dots,\end{aligned}\tag{2.16}$$

where $\kappa = \left(\frac{\lambda}{8\pi}\right)^2$. The leading n term in κ was first given in Ref. [9]. The terms up to $\mathcal{O}(\kappa^2)$ were given in Ref. [5], where the agreement with perturbative calculations was also checked at two loops ($\mathcal{O}(\kappa)$). We shall now continue the perturbative check of the semiclassical results to four and then six loops. The four-loop diagrams are shown in Fig. 1. The lozenge represents the location of the ϕ^n vertex. The extraction of the poles in ϵ from these diagrams is described in some detail in the Appendix. The results for the various

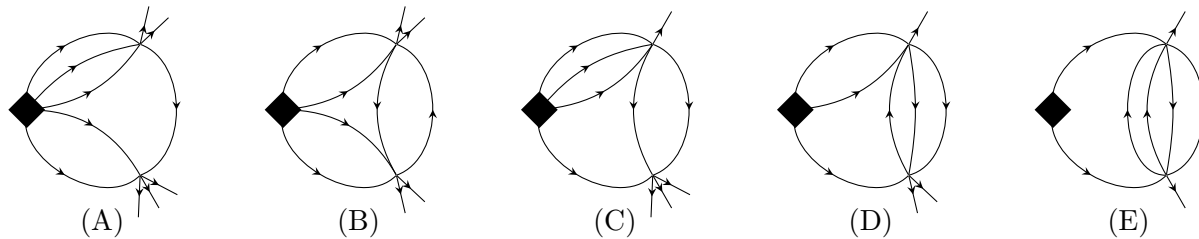


Figure 1: Four loop diagrams corresponding to γ_{ϕ^n}

diagrams in terms of a basic set of Feynman integrals is shown in Table 1 (a factor of κ^2 is also implicitly assumed for each graph). The notation for these integrals conforms to Ref. [10]. Using the results for these integrals as listed in that paper, and also recapitulated in the Appendix, the total for the four loop anomalous dimension is thus (remembering to multiply the simple pole contribution by a loop factor of four)⁴

$$\gamma_{\phi^n}^{(4)} = -\kappa^2 \frac{n(n-1)}{72} \left[9\pi^2(n-2)(n-3) + 8n^3 - 56n^2 + 272n - 456 \right].\tag{2.17}$$

⁴Eq. (2.17) represents the contribution from the graphs shown in Fig. 1. We have omitted contributions from graphs with self energy insertions on the external lines, which, however, contribute only to the term linear in n .

Graph	Result
A	$\frac{n(n-1)(n-2)(n-3)(n-4)}{144} I_4$
B	$\frac{n(n-1)(n-2)(n-3)}{32} I_{4bbb}$
C	$\frac{n(n-1)(n-2)(n-3)}{72} I_4$
D	$\frac{n(n-1)(n-2)}{8} I_4$
E	$\frac{n(n-1)}{8} \tilde{Y}$

Table 1: Four-loop results for contributions to γ_{ϕ^n}

This result can in principle also be extracted from expressions derived in Refs. [11] and [12]. Expanding in powers of $1/n$ we obtain

$$\gamma_{\phi^n}^{(4)} = -\frac{\kappa^2}{9} \left[n^5 + n^4 \left(\frac{9\pi^2}{8} - 8 \right) + \dots \right], \quad (2.18)$$

in agreement with Eq. (2.16) and Eq. (31) of [5].

We now turn to the six-loop calculation. At this loop order we focus from the outset on the contributions leading and subleading in n . The leading order six-loop contributions come solely from the diagrams depicted in Fig. 2 (of course these also produce contributions of lower order in n). Once again, the extraction of the poles in ϵ from these diagrams is described in some detail in the Appendix; the small black circles at the vertices will be explained in that context. The next-to-leading contributions six-loop contributions come from the diagrams in Fig. 2, together with the additional diagrams depicted in Fig. 3.

The resulting simple poles for each diagram are tabulated in Table 2, together with the corresponding symmetry factors. A factor of κ^3 should also be included for each diagram. For completeness, the full set of pole terms is listed in the Appendix, in Eq. (A.20).

The contribution to the six-loop anomalous dimension from the diagrams in Figs. 2, 3 is then obtained by adding the products of corresponding symmetry factors and simple poles in Table 2 and multiplying by the usual loop factor of six and a factor κ^3 . The

Graph	Symmetry Factor	Simple Pole
2(a)	$\frac{1}{1728} \frac{n!}{(n-6)!}$	$-\frac{16}{3}$
2(b)	$\frac{1}{576} \frac{n!}{(n-6)!}$	$\frac{64}{3}$
2(c)	$\frac{1}{1728} \frac{n!}{(n-6)!}$	$\frac{16}{3}$
3(a)	$\frac{1}{96} \frac{n!}{(n-5)!}$	$-\frac{2}{3}\pi^2(2 \ln 2 - 5)$
3(b)	$\frac{1}{144} \frac{n!}{(n-5)!}$	$-\frac{16}{9}(\pi^2 - 12)$
3(c)	$\frac{1}{288} \frac{n!}{(n-5)!}$	$-\frac{8}{9}(\pi^2 - 24)$
3(d)	$\frac{1}{288} \frac{n!}{(n-5)!}$	$\frac{64}{3}$
3(e)	$\frac{1}{864} \frac{n!}{(n-5)!}$	$\frac{16}{3}$
3(f)	$\frac{1}{96} \frac{n!}{(n-5)!}$	$\pi^2 \left(\frac{4}{3} \ln 2 + 2 \right)$
3(g)	$\frac{1}{192} \frac{n!}{(n-5)!}$	$\frac{2}{3}\pi^4$
3(h)	$\frac{1}{864} \frac{n!}{(n-5)!}$	$\frac{8}{9}(\pi^2 - 6)$

Table 2: Six-loop results from Figs. 2, 3

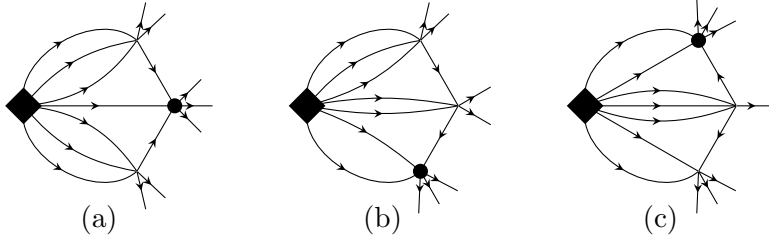


Figure 2: Six-loop diagrams for γ_{ϕ^n} contributing at leading n

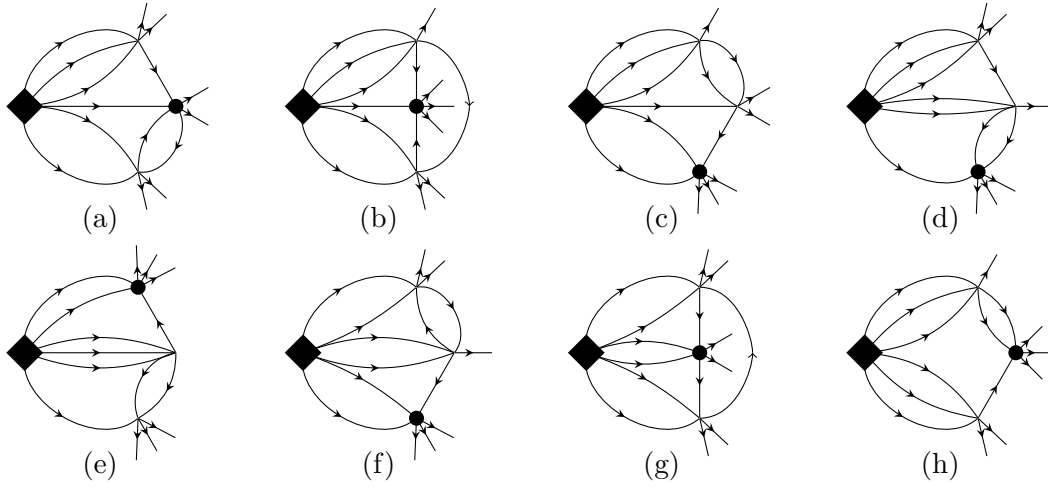


Figure 3: Additional six-loop diagrams for γ_{ϕ^n} contributing at next-to-leading n

contribution at leading and next-to-leading n is given by

$$\gamma_{\phi^n}^{(6)} = \frac{2}{9}\kappa^3 \left(n^7 + \left[-13 + \frac{10}{9}\pi^2 + \frac{3}{32}\pi^4 \right] n^6 + \dots \right), \quad (2.19)$$

in agreement with Eq. (2.16).

3 The $O(N)$ case

In the four-dimensional case the $U(1)$ computation of Ref. [5] was extended to $O(N)$ in Ref. [7]. A similar agreement between the semiclassical and perturbative calculations was found, up to three-loop order in perturbation theory. It seems natural to perform a similar extension to $O(N)$ in the case at hand, especially as the group theory and other results developed in Ref. [7] may straightforwardly be adapted to $d = 3$. Of course this represents a generalisation of the $U(1)$ calculation, since the latter may be recovered as the special case $N = 2$; but now we may also wish to consider the limit of large N , for example.

In the $O(N)$ case we have a multiplet of fields ϕ_i , $i = 1 \dots N$, and the Lagrangian is now

$$\mathcal{L} = \frac{1}{2} \partial^\mu \phi_i \partial_\mu \phi_i + \frac{g^2}{8 \times 3!} (\phi_i \phi_i)^3. \quad (3.1)$$

As shown in Ref. [7], the fixed-charge operator of charge \bar{Q} may be taken to be

$$T_{\bar{Q}} = T_{i_1 i_2 \dots i_{\bar{Q}}} \phi_{i_1} \phi_{i_2} \dots \phi_{i_{\bar{Q}}}, \quad (3.2)$$

where $T_{i_1 i_2 \dots i_{\bar{Q}}}$ is symmetric, and traceless on any pair of indices. The scaling dimension $\Delta_{T_{\bar{Q}}}$ is expanded in a similar fashion to Eq. (2.2) as

$$\Delta_{T_{\bar{Q}}} = \bar{Q} \left(\frac{d}{2} - 1 \right) + \gamma_{T_{\bar{Q}}} = \sum_{\kappa=-1} \lambda^\kappa \Delta_\kappa(g\bar{Q}). \quad (3.3)$$

As in the $U(1)$ case, we initially work in general d . The semiclassical computation of Δ_{-1} and Δ_0 proceeds in a similar manner to the $U(1)$ case, but now the chemical potential μ is related to the cylinder radius R by

$$R\mu = \frac{1}{2\sqrt{2}} \sqrt{1 + \sqrt{1 + \frac{g^2 \bar{Q}^2}{2\pi^2}}}. \quad (3.4)$$

The computation of the leading contribution is entirely analogous to the $U(1)$ case and is given by

$$\Delta_{-1}(g\bar{Q}) = g\bar{Q} F_{-1} \left(\frac{g^2 \bar{Q}^2}{2\pi^2} \right), \quad (3.5)$$

where F_{-1} is as defined in Eq. (2.5). As in the $U(1)$ case, for simplicity we give in Eq. (3.4) the result for $d = 3$. The non-leading corrections Δ_0 are once more given by the determinant of small fluctuations. There are two modes corresponding to those in the abelian case, with the dispersion relation in Eq. (2.6). In addition there are $\frac{N}{2} - 1$ ‘‘Type II’’ (non-relativistic) [8] Goldstone modes and $\frac{N}{2} - 1$ massive states with dispersion relation

$$\omega_{\pm\pm}(l) = \sqrt{J_l^2 + \mu^2} \pm \mu, \quad (3.6)$$

with J_l as defined in Eq. (2.7). We then find that Δ_0 is given by

$$\Delta_0(g\bar{Q}) = \Delta_0^{(a)}(g\bar{Q}) + \left(\frac{N}{2} - 1 \right) \Delta_0^{(b)}(g\bar{Q}), \quad (3.7)$$

where

$$\Delta_0^{(a)}(g\bar{Q}) = \frac{R}{2} \sum_{l=0}^{\infty} n_l [\omega_+(l) + \omega_-(l)]$$

$$\Delta_0^{(b)}(g\bar{Q}) = \frac{R}{2} \sum_{l=0}^{\infty} n_l [\omega_{++}(l) + \omega_{--}(l)]. \quad (3.8)$$

Here n_l defined in Eq. (2.10) is again the multiplicity of the laplacian on the d -dimensional sphere, and ω_{\pm} are defined in (2.6) but with R, μ now related by Eq. (3.4). As before, with a slight abuse of notation, after analytic continuation we replace $\Delta_0^{(a)}(g\bar{Q}), \Delta_0^{(b)}(g\bar{Q})$ by regularised forms

$$\begin{aligned} \Delta_0^{(a)}(g\bar{Q}) &= \frac{1}{4} - 3(R\mu)^2 + \frac{1}{2}\sqrt{8R^2\mu^2 - 1} + \frac{1}{2} \sum_{l=1}^{\infty} \sigma^{(a)}(l), \\ \Delta_0^{(b)}(g\bar{Q}) &= -\frac{1}{4} - (R\mu)^2 + R\mu + \frac{1}{2} \sum_{l=1}^{\infty} \sigma^{(b)}(l), \end{aligned} \quad (3.9)$$

where

$$\begin{aligned} \sigma^{(a)}(l) &= (1 + 2l)R[\omega_+(l) + \omega_-(l)] \\ &\quad - 4l(l + 1) - \left(6(R\mu)^2 - \frac{1}{2}\right), \\ \sigma^{(b)}(l) &= (1 + 2l)R[\omega_{++}(l) + \omega_{--}(l)] \\ &\quad - 4l(l + 1) - \left(2(R\mu)^2 + \frac{1}{2}\right), \end{aligned} \quad (3.10)$$

are defined once again by subtracting positive and zero powers of l in the large- l expansions of Eq. (3.8) so as to give a convergent sum in $d = 3$. Now expanding $\sigma^{(a)}(l), \sigma^{(b)}(l)$ in powers of $\frac{g^2\bar{Q}^2}{2\pi^2}$, we find

$$\begin{aligned} \sigma^{(a)}(l) &= C_{2,l} \left(\frac{g^2\bar{Q}^2}{2\pi^2}\right)^2 + C_{3,l} \left(\frac{g^2\bar{Q}^2}{2\pi^2}\right)^3 + \dots, \\ \sigma^{(b)}(l) &= \tilde{C}_{2,l} \left(\frac{g^2\bar{Q}^2}{2\pi^2}\right)^2 + \tilde{C}_{3,l} \left(\frac{g^2\bar{Q}^2}{2\pi^2}\right)^3 + \dots, \end{aligned} \quad (3.11)$$

where $C_{2,l}, C_{3,l}$ were defined in Eq. (2.14), and

$$\tilde{C}_{2,l} = -\frac{1}{128(2l+1)^2}, \quad \tilde{C}_{3,l} = \frac{16l^2 + 16l + 5}{1024(2l+1)^4}. \quad (3.12)$$

Performing the summations, and combining Eqs. (3.3) (with $d = 3$), (3.5), and (3.7)-(3.12), we find the expansion

$$\Delta_{T\bar{Q}} = \frac{\bar{Q}}{2} + \tilde{\kappa} \left[\frac{2}{3}(\bar{Q}^3 - 3\bar{Q}^2) + \mathcal{O}(\bar{Q}) \right]$$

Graph	Result
A	$\frac{\bar{Q}(\bar{Q}-1)(\bar{Q}-2)(\bar{Q}-3)(\bar{Q}-4)}{4} I_4$
B	$\frac{9}{8} \bar{Q}(\bar{Q}-1)(\bar{Q}-2)(\bar{Q}-3) \frac{1}{18} (16+N) I_{4bbb}$
C	$\frac{\bar{Q}(\bar{Q}-1)(\bar{Q}-2)(\bar{Q}-3)}{2} I_4$
D	$\frac{9}{2} \bar{Q}(\bar{Q}-1)(\bar{Q}-2) I_4$
E	$\frac{9}{2} \bar{Q}(\bar{Q}-1) \tilde{Y}$

Table 3: Four-loop results for $O(N)$ case

$$\begin{aligned}
& -\tilde{\kappa}^2 \left[4\bar{Q}^5 - \left\{ 32 - \left(4 + \frac{1}{4}N \right) \pi^2 \right\} \bar{Q}^4 + \mathcal{O}(\bar{Q}^3) \right] \\
& + \tilde{\kappa}^3 \left[48\bar{Q}^7 + \left\{ -624 + \left(\frac{136}{3} + 4N \right) \pi^2 + \frac{1}{12} (52 + N) \pi^4 \right\} \bar{Q}^6 + \mathcal{O}(\bar{Q}^5) \right] + \dots,
\end{aligned} \tag{3.13}$$

where $\tilde{\kappa} = \left(\frac{g}{8\pi} \right)^2$. We note that the $U(1)$ result in the previous section may be obtained by setting $N = 2$ and making the substitution $g^2 = \frac{1}{6} \lambda^2$.

The contributions from individual diagrams for this case are shown in Tables 3 and 4. Factors of $\tilde{\kappa}^2$ at four loops and $\tilde{\kappa}^3$ at six loops are implicit. As mentioned before, the $U(1)$ results may be recovered by setting $N = 2$ and making the substitution $g^2 = \frac{1}{6} \lambda^2$. Once again, after adding the diagrammatic contributions and including a loop factor of 4 and 6 respectively, the leading and subleading four and six loop contributions agree with the semiclassical result in Eq. (3.13). It is noteworthy that the N dependence in Eq. (3.13) involves purely powers of π^2 ; and this feature in fact appears to persist to higher orders. It would be interesting to be able to associate this with a generic topological property of the relevant Feynman diagrams.

Graph	Symmetry Factor	Simple Pole
2(a)	$\frac{1}{8} \frac{\bar{Q}!}{(\bar{Q}-6)!}$	$-\frac{16}{3}$
2(b)	$\frac{3}{8} \frac{\bar{Q}!}{(\bar{Q}-6)!}$	$\frac{64}{3}$
2(c)	$\frac{1}{8} \frac{\bar{Q}!}{(\bar{Q}-6)!}$	$\frac{16}{3}$
3(a)	$\frac{9}{4} \frac{\bar{Q}!}{(\bar{Q}-5)!} \frac{1}{432} (384 + 24N)$	$-\frac{2}{3} \pi^2 (2 \ln 2 - 5)$
3(b)	$\frac{3}{2} \frac{\bar{Q}!}{(\bar{Q}-5)!}$	$-\frac{16}{9} (\pi^2 - 12)$
3(c)	$\frac{3}{4} \frac{\bar{Q}!}{(\bar{Q}-5)!}$	$-\frac{8}{9} (\pi^2 - 24)$
3(d)	$\frac{3}{4} \frac{\bar{Q}!}{(\bar{Q}-5)!}$	$\frac{64}{3}$
3(e)	$\frac{1}{4} \frac{\bar{Q}!}{(\bar{Q}-5)!}$	$\frac{16}{3}$
3(f)	$\frac{9}{4} \frac{\bar{Q}!}{(\bar{Q}-5)!} \frac{1}{432} (384 + 24N)$	$\pi^2 \left(\frac{4}{3} \ln 2 + 2 \right)$
3(g)	$\frac{9}{8} \frac{\bar{Q}!}{(\bar{Q}-5)!} \frac{1}{432} (416 + 8N)$	$\frac{2}{3} \pi^4$
3(h)	$\frac{1}{4} \frac{\bar{Q}!}{(\bar{Q}-5)!}$	$\frac{8}{9} (\pi^2 - 6)$

Table 4: Six Loop Results for $O(N)$ case

4 Large $g\bar{Q}$

In the $U(1)$ case, the result for the anomalous dimension may be expanded for large λn and compared with the effective theory for the gapless Goldstone mode corresponding to ω_- . In the $O(N)$ case, we can do an analogous expansion for large $g\bar{Q}$. Following Ref. [5], we obtain

$$\Delta_{T_{\bar{Q}}} = \bar{t}^{\frac{3}{2}} \left[c_{3/2} + c_{1/2}\bar{t}^{-1} + c_{-1/2}\bar{t}^{-2} + \dots \right] + \left[d_0 + d_{-1}\bar{t}^{-1} + \dots \right]. \quad (4.1)$$

with $\bar{t} = \frac{\sqrt{2}g\bar{Q}}{\pi}$ and

$$c_i = \tilde{c}_i + \left(\frac{N}{2} - 1 \right) \bar{c}_i, \quad d_i = \tilde{d}_i + \left(\frac{N}{2} - 1 \right) \bar{d}_i, \quad (4.2)$$

where

$$\begin{aligned} \tilde{c}_{3/2} &\approx \frac{\pi}{6\sqrt{2}g} - 0.0653 + \mathcal{O}\left(\frac{\sqrt{2}g}{\pi}\right), \\ \tilde{c}_{1/2} &\approx \frac{\pi}{2\sqrt{2}g} + 0.2088 + \mathcal{O}\left(\frac{\sqrt{2}g}{\pi}\right), \\ \tilde{c}_{-1/2} &\approx -\frac{\pi}{4\sqrt{2}g} - 0.2627 + \mathcal{O}\left(\frac{\sqrt{2}g}{\pi}\right), \\ \tilde{d}_0 &\approx -0.0937255, \\ \tilde{d}_{-1} &\approx 0.096 + \mathcal{O}\left(\frac{\sqrt{2}g}{\pi}\right). \end{aligned} \quad (4.3)$$

and

$$\begin{aligned} \bar{c}_{3/2} &\approx -0.010417, \\ \bar{c}_{1/2} &\approx 0.052083, \\ \bar{c}_{-1/2} &\approx -0.096875, \\ \bar{d}_0 &\approx \bar{d}_1 \approx 0, \end{aligned} \quad (4.4)$$

The leading-order contributions in Eq. (4.3) follow straightforwardly from expanding Δ_{-1} in Eq. (3.5) for large $g\bar{Q}$ using Eq. (2.5). The next-to-leading order numbers, in Eqs. (4.3) and (4.4), derive from a numerical fit to Δ_0 as given by Eq. (3.8), following the procedure explained in Ref. [5] and in more detail in Ref. [6].

The values in Eqs. (4.3) were essentially given already in Ref. [5], after making allowance for the change from λn to $g\bar{Q}$. The numerical coefficients \bar{c}_i in Eq. (4.4) are therefore

the only new features of the $O(N)$ case at large $g\overline{Q}$. We note the intriguing fact that $\overline{c}_{3/2} = 5\overline{c}_{1/2}$. This fact and indeed the values of the remaining \overline{c}_i may be explained quite simply. It is convenient to consider an expansion of Δ_0 in powers of $v = R\mu$, rather than $g\overline{Q}$; of course in view of Eq. (3.4), large $g\overline{Q}$ implies large $R\mu$. We find from redoing the numerical matching

$$\Delta_0 = a_3 v^3 + a_2 v^2 + a_1 v + a_0 + \frac{a_{-1}}{v} + \frac{a_{-2}}{v^2} + \frac{a_{-3}}{v^3} + \dots, \quad (4.5)$$

with

$$a_i = \tilde{a}_i + \left(\frac{N}{2} - 1\right) \bar{a}_i, \quad (4.6)$$

where

$$\begin{aligned} \tilde{a}_3 &\approx -4.1812, \\ \tilde{a}_2 &\approx 0, \\ \tilde{a}_1 &\approx 1.6192, \\ \tilde{a}_0 &\approx -0.093725, \\ \tilde{a}_{-1} &\approx -0.09334, \\ \tilde{a}_{-2} &\approx 0.006051, \\ \tilde{a}_{-3} &\approx -0.003911, \end{aligned} \quad (4.7)$$

and

$$\begin{aligned} \bar{a}_3 &\approx -2\bar{a}_1 \approx -\frac{2}{3}, \\ \bar{a}_2 &\approx \bar{a}_0 \approx \bar{a}_{-2} \approx \bar{a}_{-4} \approx 0, \\ \bar{a}_{-1} &\approx -\frac{1}{30}, \\ \bar{a}_{-3} &\approx -0.0031746, \\ \bar{a}_{-5} &\approx -0.0011992. \end{aligned} \quad (4.8)$$

It is easy to see by expanding $R\mu$ in Eq. (2.3) that the coefficients \tilde{d}_i and \bar{d}_i in Eq. (4.1) depend only on the even powers of $R\mu$, \tilde{a}_{2j} and \bar{a}_{2j} , respectively, and indeed we see from Eq. (4.8) that the \bar{a}_{2j} and the \bar{d}_i all vanish. It is also easy to check that the \tilde{c}_i and \overline{c}_i coefficients in Eqs. (4.3) and (4.4) are derived from the odd coefficients \tilde{a}_{2j+1} and \bar{a}_{2j+1} . For instance we have

$$\overline{c}_{3/2} = \frac{1}{64}\bar{a}_3, \quad \overline{c}_{1/2} = \frac{1}{64}(3\bar{a}_3 + 16\bar{a}_1) \quad \overline{c}_{-1/2} = \frac{1}{128}(9\bar{a}_3 + 32\bar{a}_1 + 512\bar{a}_{-1}), \quad (4.9)$$

(with similar relations for \tilde{c}_i and \tilde{a}_i) which are easily verified using the values in Eqs. (4.3), (4.4), (4.7) and (4.8). The previously-noted relation $\overline{c}_{3/2} = 5\overline{c}_{1/2}$ is seen to follow from the relation $\bar{a}_3 = -2\bar{a}_1$ in Eq. (4.8). The values of the coefficients of \bar{a}_i for negative i may

now be understood as follows. Once again separating Δ_0 as in Eq. (3.8), we find from the analytic expansion of Eq. (3.9) for large v

$$\begin{aligned}\Delta_0^{(a)} &= \sum_{l=0}^{\infty} \left\{ -2l(l+1) - 3v^2 + \frac{1}{4} \right. \\ &\quad \left. + \sqrt{2}(1+2l) \left(v + \frac{1}{4}\tilde{J}_l - \frac{1}{32} \frac{2-3\tilde{J}_l^2}{v} + \frac{1}{128} \frac{\tilde{J}_l^3 - \tilde{J}_l}{v^2} \right) \right\}, \\ \Delta_0^{(b)} &= \sum_{l=0}^{\infty} \left\{ -2l(l+1) - v^2 - \frac{1}{4} \right. \\ &\quad \left. + (1+2l) \left(v + \frac{\tilde{J}_l^2}{2v} - \frac{\tilde{J}_l^4}{8v^3} + \frac{\tilde{J}_l^6}{16v^5} + \dots \right) \right\},\end{aligned}\tag{4.10}$$

where

$$\tilde{J}_l^2 = R^2 J_l^2 = l(l+1)\tag{4.11}$$

with J_l^2 as in Eq. (2.7), but with $d = 3$. We would now be able to reproduce Eq. (4.5) with Eqs. (4.7), (4.8), if we could perform the summations over l . However, it turns out that we can only make progress on this in the case of $\Delta_0^{(b)}$. Its two crucial properties appear to be the following: it has an expansion in powers of $\frac{\tilde{J}_l^2}{v^2}$, with a leading term v , and, as we explained earlier, the leading positive/zero powers in the large- l expansion have been subtracted in Eq. (3.9) (as they also were for $\Delta_0^{(a)}$, of course). An immediate consequence is that there are no negative even powers of v in $\Delta_0^{(b)}$ in Eq. (4.10), implying the vanishing of the \bar{a}_{2j} for j negative. The summations in Eq. (4.10) are all *a priori* infinite. Nevertheless, it turns out that we can obtain regularised results for those in $\Delta_0^{(b)}$ corresponding to odd powers of v . If we write

$$\zeta(s) = \sum_{l=1}^{\infty} l^{-s}\tag{4.12}$$

then we can define

$$\begin{aligned}\sum_{l=0}^{\infty} l^n &= \zeta(-n) = (-1)^n \frac{B_{n+1}}{n+1}, \quad (n > 0), \\ \sum_{l=0}^{\infty} l^0 &= \zeta(0) + 1 = B_1 + 1,\end{aligned}\tag{4.13}$$

where B_n are the Bernoulli numbers. In the second sum in Eq. (4.13), we have accounted for the fact that the series in Eq. (4.10), Eq. (4.12), start at $l = 0$, $l = 1$, respectively; of course this makes no difference in the first sum. We obtain the following expressions for the coefficients:

$$\bar{a}_1 = [-B_2 + B_1 + 1] = \frac{1}{3},$$

$$\begin{aligned}
\bar{a}_{-1} &= -\frac{1}{2} \left[-\frac{1}{2}B_4 + \frac{1}{2}B_2 \right] = \frac{1}{4} \left(\frac{1}{30} - \frac{1}{6} \right) = -\frac{1}{30}, \\
\bar{a}_{-3} &= \frac{1}{8} \left[\frac{1}{3}B_6 + B_4 \right] = -\frac{1}{8} \left[-\frac{1}{3} \cdot \frac{1}{42} + \frac{1}{30} \right] \\
&= -\frac{1}{315} \approx -0.0031746, \\
\bar{a}_{-5} &= -\frac{1}{16} \left[\frac{1}{4}B_8 + \frac{3}{2}B_6 + \frac{1}{4}B_4 \right] = \frac{1}{64} \left[\frac{1}{30} - 6\frac{1}{42} + \frac{1}{30} \right] \\
&= -\frac{1}{840} \approx -0.0011905.
\end{aligned} \tag{4.14}$$

recalling that $B_n = 0$ for n odd, except for $n = 1$. Comparing with Eq. (4.8), we find surprisingly good agreement. Turning now to \bar{a}_0 and \bar{a}_2 , the cancellation of leading powers of l in Eq. (3.9) appears to guarantee the vanishing of these coefficients as observed in Eq. (4.8), even though the ζ -function sums defined by Eq. (4.13) do not give vanishing results for the v^2 and v^0 terms in Eq. (4.10). We have checked that for other functions sharing the crucial properties mentioned above, we similarly obtain $\bar{a}_i = 0$ for $i \leq 2$ and even; and the ζ -function sums correctly give \bar{a}_i for $i \leq 1$ and odd. However, \bar{a}_3 remains a problem. There is no v^3 term in Eq. (4.10) to match the one in Eq. (4.5); though if one approximates the original sum over l in Eq. (3.8) by an integral, one easily sees the emergence of a v^3 term, with indeed the correct coefficient.

On the other hand, although the definition of $\Delta_0^{(a)}$ in Eq. (3.9) correctly subtracts the leading l^2 and l^0 terms, the large- v expansion in Eq. (4.10) does not have the other crucial property mentioned above. Consequently it contains odd powers of \tilde{J}_l (associated with negative even powers of v) and hence factors of $\sqrt{l(l+1)}$ which cannot be summed using Eq. (4.13). Furthermore, the ζ -function sums for the odd powers of v fail to agree with the results obtained in Eq. (4.7). It is then no surprise that \tilde{a}_2 and \tilde{a}_0 in Eq. (4.7) fail to vanish, as might otherwise have been expected from our experience with $\Delta_0^{(b)}$.

Nevertheless, we have succeeded in obtaining exact expressions for the “new” coefficients in the large $R\mu$, and consequently large $g\bar{Q}$, expansions in the $O(N)$ case (i.e. those coefficients which are not already present in the $U(1)$ case); albeit we have no rigorous explanation for the values of $\bar{a}_3 = -\frac{2}{3}$, $\bar{a}_2 = \bar{a}_0 = 0$.

5 Conclusions

Neutron stars, and high density quark matter can both be described in terms of a superfluid effective field theory for a Goldstone boson field [13] [14]. As explained in Ref. [5], relevant issues may also be addressed in terms of the relativistic theory of a complex scalar field ϕ with $\left(\frac{\lambda}{3!}\right)^2 (\phi^* \phi)^3$ interactions, in $d = 3 - \epsilon$ dimensions. This theory has a conformal fixed

point (for small ϵ) at

$$\left(\frac{\lambda}{3!}\right)^2 = \frac{3}{7}\epsilon. \quad (5.1)$$

In this paper we have extended the calculation of the anomalous dimension of the operator ϕ^n embarked upon in Ref. [5] from two loops to four and six loops. We continue to find agreement between the straightforward perturbative (in λ^2) calculation and the results of a semiclassical calculation, along the lines explained in Ref. [6]. This agreement interpolates between large and small λn .

We performed similar calculations for an $O(N)$ theory with $(\phi^i\phi^i)^3$ interactions, which includes the $U(1)$ case described above as the special case $N = 2$. Here both semiclassical and perturbative approaches were pursued in Ref [7], for $(\phi^i\phi^i)^2$ theory in $d = 4 - \epsilon$, which similarly has a conformal fixed point with a coupling constant of $O(\epsilon)$. It turns out to be quite straightforward to adapt these calculations to the $d = 3 - \epsilon$ case, and once again we find that the perturbative and semiclassical approaches interpolate seamlessly into one another. The conformal fixed point is crucial to the semiclassical discussion. In the large- N limit, the coupling must be rescaled, and the conformal fixed point is changed so the discussion would require modification⁵; we do not pursue this issue here. Finally in the $O(N)$ case we have shown how to compute exactly the N -dependent parts of the coefficients in the large charge expansion.

Acknowledgements

We thank John Gracey and Hugh Osborn for conversations and Andrei Kataev and Diego Rodriguez-Garcia for correspondence. DRTJ thanks the Leverhulme Trust for the award of an Emeritus Fellowship. This research was supported by the Leverhulme Trust, STFC and by the University of Liverpool.

A Full diagram results

In this appendix we explain in some detail how we have derived our perturbative results. We start with a pedagogical description of the four-loop calculation; the techniques are well-known to high-loop experts but maybe not to the wider community and not in the three-dimensional context.

We define the result of the generic one-loop integral by the “ G -function” $G(a, b)$ [15], so that

$$G(a, b) = \int d^d k \frac{p^{2(a+b-\frac{d}{2})}}{k^{2a}(p-k)^{2b}} = \frac{\Gamma(a+b-\frac{d}{2})\Gamma(\frac{d}{2}-a)\Gamma(\frac{d}{2}-b)}{(4\pi)^{\frac{d}{2}}\Gamma(a)\Gamma(b)\Gamma(d-a-b)}. \quad (A.1)$$

⁵The fixed point structure in $d = 3$ at large N is explored in Ref. [12]

The first divergence appears in the two-loop integral G_2 depicted in Fig. 4, and given by

$$G_2 = G_1 G \left(2 - \frac{1}{2}d, 1 \right) \quad (\text{A.2})$$

where for convenience we denote the basic one-loop bubble by $G_1 = G(1, 1)$. The pole term is given by

$$I_2 = \hat{K}[G_2] = \frac{1}{64\pi^2} \frac{2}{\epsilon}, \quad (\text{A.3})$$

where \hat{K} denotes the operation of extracting the divergent part. Note that our convention in this paper is that G denotes the full momentum integral and I the corresponding local counterterm (after subtracting subdivergences where necessary; see later). We are using minimal subtraction, so the counterterm is purely divergent. In a slight misuse of notation, G will often be used to refer both to the graph and to the corresponding Feynman integral.

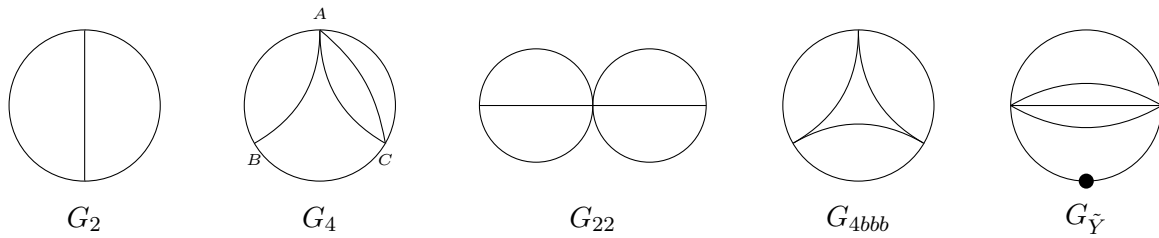


Figure 4: Two- and four-loop momentum integrals

The four-loop momentum integrals are also depicted in Fig. 4. The Feynman graphs corresponding to all diagrams considered in this paper (two, four and six loop) are logarithmically divergent and consequently the extraction of the counterterms may be simplified using “infra-red (IR) rearrangement”.⁶ This involves judiciously setting selected external momenta to zero, leaving a single momentum entering at one vertex and leaving at another, in order to obtain a more tractable integral. It will be useful to focus on G_4 for our pedagogical introduction. For convenience we have labelled the vertices of G_4 in Fig. 4 by A, B, C . We first consider the case where a momentum enters at A and leaves at B . The basic momentum integral is given by

$$G_4 = G_1 G_2 G \left(2 - \frac{1}{2}d, 4 - d \right). \quad (\text{A.4})$$

There is also a divergent two-loop subgraph, with a divergence I_2 , which needs to be subtracted to obtain a local result. We obtain

$$I_4 = \hat{K}\overline{R}[G_4] = \hat{K} \left[G_2 \left\{ G_1 G \left(2 - \frac{1}{2}d, 4 - d \right) - I_2 \right\} \right] = \frac{1}{(64\pi^2)^2} \frac{1}{\epsilon^2} (-2 + 4\epsilon). \quad (\text{A.5})$$

The process of correctly subtracting the subdivergences is here denoted \overline{R} . For more details see Ref. [18] where the procedure is well explained (with reference to the four-dimensional

⁶This technique was used in very early “multi-loop” calculations [16], [17].

case). In general there may be several distinct ways of implementing the IR rearrangement. Any IR rearrangement which avoids the introduction of spurious IR divergences will give the same result for the final counterterm, after making the appropriate subtractions. In the case of I_4 , for instance, we may also consider the case where a momentum enters at C and leaves at B . The basic momentum integral is then given by

$$G'_4 = G_1 G_2 G \left(5 - \frac{3}{2}d, 1 \right), \quad (\text{A.6})$$

and we now have

$$I_4 = \hat{K} \overline{R}[G'_4] = \hat{K} \left[G_2 \left\{ G_1 G \left(5 - \frac{3}{2}d, 1 \right) - I_2 \right\} \right] = \frac{1}{(64\pi^2)^2} \frac{1}{\epsilon^2} (-2 + 4\epsilon). \quad (\text{A.7})$$

As emphasised earlier, the same result is obtained for the counterterm I_4 . In general, in the process of IR rearrangement, the same entry and exit points must be used for the subtracted diagrams as for the original. For a different IR rearrangement of a given diagram, the pole terms for the original diagram and the subtracted diagrams will typically be individually different, but will combine to give the same total counterterm. In the current case, the subtractions are the same for the two IR rearrangements. The same overall result is nevertheless obtained for the pole term since both G_4 and G'_4 also have the same poles, though of course differ in their finite parts.

There is a final possible IR rearrangement, where the momentum enters at A and leaves at C . This requires a more careful treatment. In four dimensions one is familiar with the basic IR divergence from a double propagator; in the current case of three dimensions, the basic IR divergence is a double propagator followed by a single one, as shown in Fig. 5. This structure leads to an effective propagator

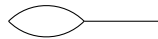


Figure 5: Basic IR-divergent structure

$$G_1 \frac{1}{(p^2)^{3-\frac{1}{2}d}} \quad (\text{A.8})$$

where the IR divergence in three dimensions is clearly revealed. It appears in this third IR rearrangement which consequently leads to a spurious IR divergence. We may avoid this spurious divergence by using the \overline{R}^* procedure, which augments the \overline{R} procedure with a subtraction for the IR divergences [19]. We start by considering the basic two-loop IR-divergent diagram in Fig. 6. This is given by

$$G_1 G \left(1, 3 - \frac{1}{2}d \right) \sim \frac{1}{64\pi^2} \left(-\frac{2}{\epsilon} \right); \quad (\text{A.9})$$

the divergence coming from $\Gamma(d-3)$ where the positive sign for d signals the infra-red nature of the divergence. The IR subtraction for this simple, single IR divergence is consequently

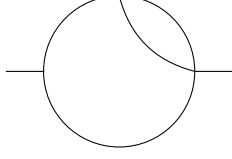


Figure 6: Two-loop IR-divergent integral

to replace Eq. (A.8) by

$$\left(G_1 \frac{1}{(p^2)^{3-\frac{1}{2}d}} + \frac{2}{64\pi^2\epsilon} \delta(p) \right). \quad (\text{A.10})$$

The IR divergence is cancelled in Fig. 6 when (A.10) is used to replace (A.8). Just as we saw earlier for the case of IR rearrangement combined with the standard \overline{R} procedure, the same process must be applied to the subtracted diagrams. Expressed diagrammatically, denoting the IR-subtracted propagator of Eq. (A.10) by a line with a box, we have

$$\begin{aligned} I_4 &= \hat{K} \left[\text{Diagram 1} - I_2 \right] \\ &= \hat{K} \left[\text{Diagram 2} + \frac{2}{64\pi^2\epsilon} \text{Diagram 3} - I_2 \text{Diagram 4} - \frac{2}{64\pi^2\epsilon} I_2 \right] \\ &= \hat{K} \left[G_1 G_2 G(3 - \frac{1}{2}d, 3 - d) + \frac{2}{64\pi^2\epsilon} G_2 - \frac{2}{64\pi^2\epsilon} I_2 \right]. \end{aligned} \quad (\text{A.11})$$

Here we denote the momentum entrance and exit points by a small black circle. A diagram with a single black circle has coincident momentum entrance and exit points and vanishes in dimensional regularisation. Once again, the same result is obtained for I_4 .

The corresponding pole terms for the remaining four-loop diagrams in Fig. 4 are given by

$$\begin{aligned} I_{22} &= \hat{K} \overline{R}[G_{22}] = \hat{K} \overline{R}[G_2^2] = \hat{K}[G_2(G_2 - 2I_2)] = \frac{1}{(64\pi^2)^2} \frac{1}{\epsilon^2} (-4), \\ I_{4bbb} &= \hat{K}[G_{4bbb}] = \hat{K}[G_1^3 G(4 - d, 2 - \frac{1}{2}d)] = \frac{1}{(64\pi^2)^2} \frac{1}{\epsilon} \pi^2, \\ \tilde{Y} &= \hat{K}[G_1^2 G(2, 2 - \frac{1}{2}d) G(4 - d, 2 - \frac{1}{2}d)] = \frac{1}{(64\pi^2)^2} \left(-\frac{2}{\epsilon} \right), \end{aligned} \quad (\text{A.12})$$

where G_{22} and G_{4bbb} are implicitly defined in terms of G -functions.

We now turn to the six-loop computation, for which the diagrams are shown in Figs. 2 and 3. These are again logarithmically divergent. Once again we use IR rearrangement,

so that we retain just a single incoming and outgoing momentum; in all our examples, this momentum may be thought of as entering at the ϕ^n vertex (i.e. the lozenge) since it turns out that this ensures wherever possible that the result may readily be expressed in terms of G -functions. The momentum leaves at the vertex marked by the small black circle. As observed earlier in the case of I_4 , the choice of momentum entrance and exit is not unique; but once made, must also be used for the subtracted diagrams. We have made the choice of momentum exit so as (for simplicity) where possible to avoid introducing infra-red divergences, either in the six-loop diagram itself or in its subtractions ; even though such IR divergences may be accommodated using the \overline{R}^* procedure. In the case of diagrams with a structure such as Fig. 5, the potential IR divergence may be avoided by choosing the central vertex in Fig. 5 as the exit for the momentum. It will be observed that this has been done in Fig. 2(b) and Figs. 3(f), (h). Less obviously, the choice of momentum exit in Fig. 3(b) has been made to avoid an IR divergence in the two-loop subtracted diagram. The process of infra-red rearrangement also reduces the number of independent integrals; for instance, with the choice of momentum exit indicated, Figs. 3(e) and 2(c) correspond to the same integral, despite the structure Fig. 5 being reversed in the latter diagram. Figs. 3(d) and 2(b) look different, since the lower single loop is on different sides of the momentum exit point. However, either of the alternative IR rearrangements using one of the other $(\phi\phi^*)^3$ vertices as exit would make the pair of diagrams look identical, and therefore would demonstrate that Figs. 3(d) and 2(b) produce the same counterterm after subtractions. Of course we could have used one of those alternative IR rearrangements, but at the expense of being obliged to use the (slightly more complicated) \overline{R}^* procedure. In all the cases mentioned so far, IR rearrangement leads to graphs which may easily be evaluated in terms of G -functions. For those where the simple \overline{R} procedure is sufficient, we find

$$\begin{aligned}
I_{2a} &= \hat{K}[G_2^2 G(4-d, 1)G(5 - \frac{3}{2}d, 4-d) - 2I_2 G_4 - I_{22} G_2], \\
I_{2b} &= I_{3d} = \hat{K}[G_1 G_4 G(2 - \frac{1}{2}d, 7-2d) - I_2 G_4 - I_4 G_2], \\
I_{3a} &= \hat{K}[G_1^2 G_2 G(4-d, 1)G(5 - \frac{3}{2}d, 4-d) - I_2 G_{4bbb}], \\
I_{3c} &= \hat{K}[G_1^2 G_2 G(5 - \frac{3}{2}d, 1)G(2 - \frac{1}{2}d, 7-2d) - I_2 G_4 - I_4 G_2], \\
I_{3f} &= \hat{K}[G_1^4 G(4-d, 2 - \frac{1}{2}d)G(2 - \frac{1}{2}d, 7-2d) - I_{4bbb} G_2], \\
I_{3h} &= \hat{K}[G_2^2 G_1 G(5 - \frac{3}{2}d, 4-d) - I_2 G_4 - I_2 G'_4 - I_{22} G_2],
\end{aligned}
\tag{A.13}$$

Here we use I_{2a} (for instance) to represent the counterterm resulting (after subtraction of subdivergences) from the Feynman integral G_{2a} corresponding to Fig. 2(a), just as I_4 results from G_4 . We shall give a complete list of explicit expressions for the pole terms later, after discussing the range of general procedures required for the different classes of diagram. We emphasise that, as explained earlier, the expression for I_{3d} in terms of diagram plus subtractions for the IR rearrangement shown in Fig. 3(d) would be different from that shown explicitly for I_{2b} , but the final total would be the same. In just one instance, Fig. 2(c) (or equivalently Fig. 3(e)), the process of IR rearrangement inevitably

introduces infra-red divergences due to the presence of two IR-divergent structures of the form Fig. 5. One of these must then be dealt with using the \overline{R}^* operation [19] explained earlier in the context of I_4 . We find

$$\begin{aligned}
I_{2c} &= \hat{K} \left[\text{Diagram 1} - I_2 \text{Diagram 2} - I_4 \text{Diagram 3} - I_4 \text{Diagram 4} \right] \\
&= \hat{K} \left[\text{Diagram 1} + \frac{2}{64\pi^2\epsilon} \text{Diagram 5} \right. \\
&\quad - I_2 \text{Diagram 2} - \frac{2}{64\pi^2\epsilon} I_2 \text{Diagram 3} - I_4 \text{Diagram 4} \\
&\quad \left. - I_4 \text{Diagram 6} - I_4 \frac{2}{64\pi^2\epsilon} \right] \\
&= \hat{K} \left[\left\{ G_1^2 G_2 G \left(3 - \frac{1}{2}d, 3 - d \right) G \left(2 - \frac{1}{2}d, 7 - 2d \right) + \frac{2}{64\pi^2\epsilon} G_4 \right\} \right. \\
&\quad \left. - \frac{2}{64\pi^2\epsilon} I_2 G_2 - I_4 G_2 - I_4 \frac{2}{64\pi^2\epsilon} \right]. \tag{A.14}
\end{aligned}$$

Once again, diagrams with a single black circle have coincident momentum entrances and exits and vanish in dimensional regularisation.

In a couple of cases, namely Figs. 3(b) and 3(g), there is no IR rearrangement which leads simply to an expression in terms of G -functions, and we need to use an identity [20] derived using the “integration by parts” trick [21] [22], which enables us to simplify integrals of the form shown in Fig. 7 which occur as substructures in these graphs. In this diagram, α_i , $i = 1 \dots 5$, represent the weights of the corresponding propagators. This identity is given here in diagrammatic form.

$$\begin{aligned}
(d - \alpha_1 - \alpha_4 - 2\alpha_5) \text{Diagram 7} &= \alpha_1 \text{Diagram 8} - \alpha_1 \text{Diagram 9} \\
&\quad + \alpha_4 \text{Diagram 10} - \alpha_4 \text{Diagram 11} \tag{A.15}
\end{aligned}$$

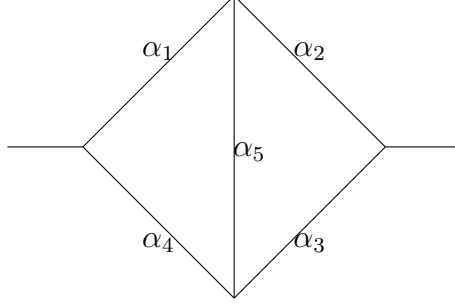


Figure 7: Diagram

Here a \pm indicates that the weight has been increased/decreased by 1, relative to the weights in Fig. 7. After performing simple one- and two-loop integrals, Figs. 3(b) and

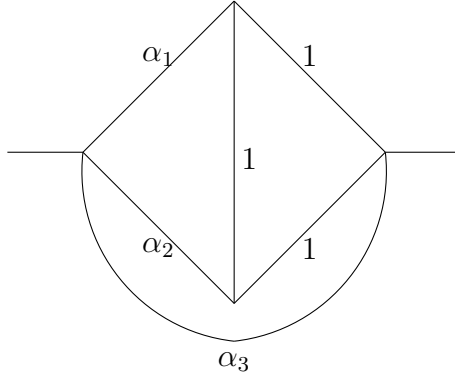


Figure 8: Diagram

(g) lead to integrals of the diagrammatic form shown in Fig. 8, which will be denoted $H(\alpha_1, \alpha_2, \alpha_3)$. It is clear that this is a special case of a diagram formed by adding an extra line joining the left and right vertices of Fig. 7. The identity in Eq. (A.15) may therefore be applied. In this special case, in each diagram on the right-hand side of Eq. (A.15) a propagator is cancelled, contracting two vertices and leaving a diagram which may easily be evaluated in terms of G -functions. We obtain diagrammatically

$$\begin{aligned}
 (d - \alpha_1 - \alpha_2 - 2)H(\alpha_1, \alpha_2, \alpha_3) = & \alpha_1 \left[\text{Diagram 1} - \text{Diagram 2} \right] \\
 & + \alpha_2 \left[\text{Diagram 3} - \text{Diagram 4} \right], \quad (\text{A.16})
 \end{aligned}$$

or, in terms of G -functions

$$H(\alpha_1, \alpha_2, \alpha_3) = \frac{G(1, 1)}{d - \alpha_1 - \alpha_2 - 2} \left[-\alpha_1 G(\alpha_1 + 1, \alpha_2) G(\alpha_1 + \alpha_2 + 3 - d, \alpha_3) \right.$$

$$\begin{aligned}
& + \alpha_1 G(\alpha_1 + 1, \alpha_3) G(\alpha_1 + \alpha_3 + 1 - \frac{1}{2}d, \alpha_2 + 2 - \frac{1}{2}d) \\
& - \alpha_2 G(\alpha_2 + 1, \alpha_1) G(\alpha_1 + \alpha_2 + 3 - d, \alpha_3) \\
& + \alpha_2 G(\alpha_2 + 1, \alpha_3) G(\alpha_2 + \alpha_3 + 1 - \frac{1}{2}d, \alpha_1 + 2 - \frac{1}{2}d) \Big]. \quad (\text{A.17})
\end{aligned}$$

The diagrams Fig. 3(b) and (g) may therefore be evaluated. Their subtractions are perfectly standard, and we obtain for the pole terms

$$\begin{aligned}
I_{3b} &= \hat{K} \bar{R}[G_{3b}] = \hat{K} [G_2 G_1 H(3 - d, 2 - \frac{1}{2}d, 1) - I_2 G_4 - I_4 G_2], \\
I_{3g} &= \hat{K} \bar{R}[G_{3g}] = \hat{K} [G_1^3 H(2 - \frac{1}{2}d, 2 - \frac{1}{2}d, 2 - \frac{1}{2}d)]. \quad (\text{A.18})
\end{aligned}$$

Finally we can give the full set of pole terms. The final results for the pole terms for the diagrams in Fig. 2 are

$$\begin{aligned}
(64\pi^3)^3 I_{2a} &= \frac{8}{3} \frac{1}{\epsilon^3} (1 - 2\epsilon - 2\epsilon^2), \\
(64\pi^3)^3 I_{2b} &= \frac{4}{3} \frac{1}{\epsilon^3} (1 - 6\epsilon + 16\epsilon^2), \\
(64\pi^3)^3 I_{2c} &= \frac{8}{3} \frac{1}{\epsilon^3} (1 - 4\epsilon + 2\epsilon^2); \quad (\text{A.19})
\end{aligned}$$

and the results for the diagrams in Fig. 3 are

$$\begin{aligned}
(64\pi^3)^3 I_{3a} &= -\frac{2}{3} \frac{1}{\epsilon^2} \pi^2 [1 + (2 \ln 2 - 5)\epsilon], \\
(64\pi^3)^3 I_{3b} &= -\frac{4}{3} \frac{1}{\epsilon^3} \left[1 - 6\epsilon - \frac{4}{3} (\pi^2 - 12)\epsilon^2 \right], \\
(64\pi^3)^3 I_{3c} &= \frac{4}{3} \frac{1}{\epsilon^3} \left[1 - 6\epsilon - \frac{2}{3} (\pi^2 - 24)\epsilon^2 \right], \\
I_{3d} &= I_{2b}, \\
I_{3e} &= I_{2c}, \\
(64\pi^3)^3 I_{3f} &= \frac{1}{\epsilon^2} \pi^2 \left[-\frac{4}{3} + \left(\frac{4}{3} \ln 2 + 2 \right) \epsilon \right], \\
(64\pi^3)^3 I_{3g} &= \frac{2}{3} \frac{1}{\epsilon} \pi^4, \\
(64\pi^3)^3 I_{3h} &= \frac{8}{3} \frac{1}{\epsilon^3} \left[1 - 2\epsilon + \frac{1}{3} (\pi^2 - 6)\epsilon^2 \right]. \quad (\text{A.20})
\end{aligned}$$

We notice that it is only primitive diagrams (which have no divergent subdiagrams and therefore only simple pole divergences) which give simple poles with a single order of transcendentality; namely I_{4bbb} in Eq. (A.12) and I_{3g} in Eq. (A.20). These produce simple poles with the maximal order of transcendentality for the corresponding loop order: π^2 at

four loops and π^4 at six loops. We note that the diagrams in Fig. 3 are all topologically identical to diagrams contributing to the six-loop β -function for the $O(N)$ scalar theory, which was computed in Ref. [23], and consequently the corresponding counterterms were computed in that paper; but unfortunately results for individual diagrams are not listed explicitly there.

References

- [1] I. Jack, D. R. T. Jones and C. Poole, “Gradient flows in three dimensions,” JHEP **1509** (2015) 061, [arXiv:1505.05400 [hep-th]].
- [2] L. V. Avdeev, G. V. Grigorev and D. I. Kazakov, Nucl. Phys. B **382** (1992), 561-580 doi:10.1016/0550-3213(92)90659-Y
- [3] L. V. Avdeev, D. I. Kazakov and I. N. Kondrashuk, “Renormalizations in supersymmetric and nonsupersymmetric nonabelian Chern-Simons field theories with matter,” Nucl. Phys. B **391** (1993), 333-357 doi:10.1016/0550-3213(93)90151-E
- [4] I. Jack and C. Poole, “ a -function in three dimensions: Beyond the leading order,” Phys. Rev. D **95** (2017) no.2, 025010 doi:10.1103/PhysRevD.95.025010 [arXiv:1607.00236 [hep-th]].
- [5] G. Badel, G. Cuomo, A. Monin and R. Rattazzi, “Feynman diagrams and the large charge expansion in $3 - \varepsilon$ dimensions,” Phys. Lett. B **802** (2020) 135202 [arXiv:1911.08505 [hep-th]].
- [6] G. Badel, G. Cuomo, A. Monin and R. Rattazzi, “The epsilon expansion meets semiclassicals”, JHEP **11** (2019) 110 [arXiv:1909.01269[hep-th]].
- [7] O. Antipin, J. Bersini, F. Sannino, Z. Wang and C. Zhang, “Charging the $O(N)$ model,” [arXiv:2003.13121 [hep-th]].
- [8] H. B. Nielsen and S. Chadha, “On how to count Goldstone bosons,” Nucl. Phys. B **105** (1976), 445-453
- [9] G. Arias-Tamargo, D. Rodriguez-Gomez and J. G. Russo, “The large charge limit of scalar field theories and the Wilson-Fisher fixed point at $\epsilon = 0$,” JHEP **10** (2019), 201 doi:10.1007/JHEP10(2019)201 [arXiv:1908.11347 [hep-th]].
- [10] J. A. Gracey, I. Jack, C. Poole and Y. Schröder, “ a -function for $N = 2$ supersymmetric gauge theories in three dimensions,” Phys. Rev. D **95** (2017) no.2, 025005 [arXiv:1609.06458 [hep-th]].

- [11] J. O’Dwyer and H. Osborn, “Epsilon expansion for multicritical fixed points and exact renormalisation group equations,” *Annals Phys.* **323** (2008), 1859-1898 doi:10.1016/j.aop.2007.10.005 [arXiv:0708.2697 [hep-th]].
- [12] H. Osborn and A. Stergiou, “Seeking fixed points in multiple coupling scalar theories in the ϵ expansion,” *JHEP* **05** (2018), 051 doi:10.1007/JHEP05(2018)051 [arXiv:1707.06165 [hep-th]].
- [13] D.T. Son, “Low-energy quantum effective action for relativistic superfluids”, hep-ph/0204199.
- [14] Alberto Nicolis, Riccardo Penco, Federico Piazza and Riccardo Rattazzi, , “Zoology of condensed matter: Framids, ordinary stuff, extra-ordinary stuff”, *JHEP* **06** (2015) 105 [arXiv:1501.03845 [hep-th]].
- [15] K. G. Chetyrkin, A. L. Kataev and F. V. Tkachov, “New approach to evaluation of multiloop Feynman integrals: the Gegenbauer polynomial x-space technique,” *Nucl. Phys. B* **174** (1980), 345-377 doi:10.1016/0550-3213(80)90289-8
- [16] D.R.T. Jones, “Two-loop diagrams in Yang-Mills theory”, *Nucl. Phys. B***75** (1974) 531.
- [17] William E. Caswell, *Phys. Rev. Lett.* **33** (1974) 244, “Asymptotic behavior of non-abelian gauge theories to two-loop order”.
- [18] H. Kleinert and V. Schulte-Frohlinde, “Critical properties of ϕ^4 -theories”, World Scientific (2001) .
- [19] K.G. Chetyrkin and F.V. Tkachov, “Infrared R operation and ultraviolet counterterms in the MS scheme”, *Phys. Lett. B* **114** (1982) 240; K.G. Chetyrkin and V.A. Smirnov, “R* operation corrected”, *Phys. Lett. B* **144** (1984) 419.
- [20] J. A. Gracey, “Large N_f quantum field theory,” *Int. J. Mod. Phys. A* **33** (2019) no.35, 1830032 doi:10.1142/S0217751X18300326 [arXiv:1812.05368 [hep-th]].
- [21] F. V. Tkachov “A theorem on analytical calculability of four loop renormalization group functions,” *Phys. Lett. B* **100** (1981), 65-68 doi:10.1016/0370-2693(81)90288-4
- [22] K. G. Chetyrkin and F. V. Tkachov, “Integration by parts: the algorithm to calculate beta functions in 4 loops,” *Nucl. Phys. B* **192** (1981), 159-204 doi:10.1016/0550-3213(81)90199-1
- [23] J. S. Hager, “Six-loop renormalization group functions of O(n)-symmetric ϕ^6 -theory and ϵ -expansions of tricritical exponents up to ϵ^3 ,” *J. Phys. A* **35** (2002), 2703-2711 doi:10.1088/0305-4470/35/12/301